Combustion and Flame 200 (2019) 53–59

Contents lists available at ScienceDirect

Combustion and Flame

journal homepage: www.elsevier.com/locate/combustflame

Triisobutylaluminum additive for liquid hydrocarbon burn enhancement

Philip M. Guerieri[a], Rohit J. Jacob[a], Dylan J. Kline[a], Andrew Kerr[b], Dennis Mayo[b], Edward E. Foos[b], Michael R. Zachariah[a,*]

[a] University of Maryland, College Park, MD 20740, United States
[b] Naval Surface Warfare Center – Indian Head Division, Indian Head, MD 20640, United States

ARTICLE INFO

Article history:
Received 16 April 2018
Revised 8 June 2018
Accepted 24 September 2018

Keywords:
Droplet combustion
Hydrocarbons
Aluminum
Organoaluminum

ABSTRACT

Metallizing hydrocarbons has received renewed attention as a potential means to increase energy density and burn rate. Particle agglomeration however, is a significant concern, impeding both performance as well as practical implementation due to system fouling. Achieving a metallized hydrocarbon without nanoparticles in suspension would avoid particle agglomeration problems. Previous proof-of-concept work with highly reactive organometallic Al-based clusters stabilized by ligands and dissolved in a hydrocarbon showed such a scheme is not only possible, but the decreased size of the cluster molecules relative to nanoparticles substantially increases reactivity and at least an order of magnitude less active aluminum. To increase understanding of how such burning rate effects manifest with dissolved aluminum, a higher valency alkyl aluminum historically used as a hypergol, triisobutylaluminum (IBu_3Al), is dissolved in toluene and isolated droplet combustion is characterized showing up to 60% burning rate increase with 810 mM IBu_3Al relative to that of pure toluene attributed specifically to the aluminum content of the additive molecule. Flame emission spectroscopy observing AlO emission supports the vital role of gas eruption and droplet disruption to transport additives into the flame.

1. Introduction

Metallizing liquid fuels and propellants have the potential to increase their net volumetric energy density thereby improving payload capabilities in volume-limited propulsion systems [1]. Addition of micron-sized metal particles to hydrocarbons, however has proved to be detrimental to combustion efficiency and single-droplet burning rates as the relatively slow-burning metal particles tend to ignite near liquid burn-out and two-phase losses can decrease specific impulse [2,3]. Research into metal/hydrocarbon incorporation has been revitalized with the emergence of nanoscale control of metal particles, and the resulting improvements in the reaction rates and ignition delays of nanometals versus micron-sized analogs [4,5]. This demonstration that the physical form of the metal drastically affects its combustion behavior has motivated consideration of metallizing hydrocarbons with soluble aluminum-containing molecules. To evaluate this concept, Guerieri et al. dissolved AlBr clusters stabilized by triethylamine ligands with aluminum in a low valency state ($[AlBrNEt_3]_4$) in a toluene/ether co-solvent. The resulting free-droplet combustion studies showed that relatively low concentrations of the material increase the burning rate of the fuel droplets compared to nanoaluminum [6].

Organoaluminum compounds comprise a similar opportunity to dissolve an aluminum component into a hydrocarbon and have been used to formulate hypergolic fuels [7]. Aluminum-based metal clusters e.g. $[AlBrNEt_3]_4$, are difficult to synthesize and maintain since they suffer from air and temperature sensitivity. While they are similarly air-sensitive and pyrophoric, alkylaluminum compounds, e.g. triisobutylaluminum (IBu_3Al), are commercially available and thermally stable, therefore providing an opportunity to contextualize the demonstrated effects of $[AlBrNEt_3]_4$, despite the higher oxidation number of Al in IBu_3Al. In this study, IBu_3Al was dissolved in toluene to investigate the effects of the hydrocarbon-soluble trialkylaluminum molecule on the free-droplet burning rate and combustion behavior relative to a nitrogen-centered control molecule, triisobutylamine (iBu_3N).

2. Experimental

A free-droplet combustion apparatus described in previous studies [6,8,9] was employed to evaluate burning rate effects of additives, in which a 600 micron droplet is released from a capillary needle into an oxygen environment and ignited with pilot

* Corresponding author.
E-mail address: mrz@umd.edu (M.R. Zachariah).

https://doi.org/10.1016/j.combustflame.2018.09.023
0010-2180/

flames (apparatus sketch provided in Supplemental Information). Oxygen is used to ensure complete droplet combustion within the apparatus. Droplet shedding off the end of the vertical capillary is achieved with nitrogen flow through a ~2 mm diameter glass shroud around the capillary at the top of the tower. Droplets are generated approximately 3 times per second and maintain separation of approximately 6 inches to prevent combustion interference. Two high-speed cameras are used to record the flame emission of the falling droplet (to measure burning time) and initial diameter of the droplet at ignition, from which a burning rate constant for each droplet can be estimated by the ratio of initial droplet diameter squared to the burning time according to Eq. (1) and the rates of 10–20 droplets averaged to estimate the burning rate of the sample.

$$K \cong \frac{{D_0}^2}{t_{\text{Burn}}} \tag{1}$$

An additional camera configuration was also used herein to gather magnified video of combusting droplets with a color high-speed camera concurrently with time-resolved emission spectroscopy between 475 nm and 500 nm. In this configuration (sketch provided in Supplemental Information), the camera and collection fiber are mounted on a vertical translation stage which is free to fall parallel to the tower, significantly lengthening the data collection times relative to the diagnostics mounted statically with droplets passing. The second camera is used to image the falling diagnostic stage and falling droplets relative to the tower axis so that the ignition time of any droplet captured in the field of view of the magnified camera and spectrometer is known. The initial diameter of the droplets is not measured in this configuration and therefore burning time data is not normalized by droplet diameter which can fluctuate +/− 50 microns. Magnified videos from the camera on the falling diagnostics stage are used to estimate spatially resolved soot/particle temperature with a three-color ratio pyrometry method described by Densmore et al. [10] using a Vision Research Phantom M110 color high-speed camera. Raw pixel values are extracted from each video frame using MATLAB, the Bayer filter array is demosaiced in red, green, and blue channels, and three color-channel ratios are calculated. Using Planck's Law, a gray-body assumption for an optically thin flame ($\varepsilon \sim 1/\lambda$) [11], and calibration by a Newport Oriel 67,000 Series blackbody infrared light source, temperature at each pixel is estimated by matching experimental color ratios to calibrated theoretical ratios as functions of temperature according to Eq. (2) using ratio calibration factors C_{gr}, C_{bg}, and C_{br} (0.952, 0.888. and 0.847 respectively, assumed valid from 773–4773 K), channel gain (ψ_i), emissivity (ε), and channel spectral response (χ_i).

$$\left(\frac{I_i}{I_j}\right) = C_{ij}\frac{\psi_i \int L(\varepsilon,\lambda,T)\chi_i(\lambda)d\lambda}{\psi_j \int L(\varepsilon,\lambda,T)\chi_j(\lambda)d\lambda} \tag{2}$$

Time-resolved emission spectra collected simultaneously with the high-speed video from the falling diagnostics stage senses atomic emission of excited AlO species in the droplet flames as an indication of aluminum oxidation. The in-house assembled spectrometer is described by Jacob et al. [12] and consists of a 1 m collection optical fiber, a 0.5 m spectroscope (Acton SP 500i) with a 1800 lines/mm grating to disperse the light between 473 and 502 nm to detect an AlO emission peak at 484 nm, and a 32-channel PMT array interfaced with a high-speed data acquisition system (Vertilon IQSP 580). The wavelength calibration was performed using a Mercury lamp (Newport) and the system sensitivity was calibrated using a black body furnace (Newport) in the range of 1200–1500 K and a high-temperature tungsten-halogen lamp (Avantes HAL-CAL) at 2440 K. The sampling rate of the acquisition system was set at 5000 Hz, sufficient to resolve emissions from sub-millisecond disruptions in the droplet flames.

A nitrogen-centered control (IBu_3N) was tested to assess the role of the Al atom in IBu_3Al aside from effects of the carrier butyl groups. Since IBu_3N features a higher boiling point than IBu_3Al, benzene was also used as an Al-free control representing a hydrocarbon with a similar boiling point to IBu_3Al. Both controls were tested at equi-molar concentrations relative to IBu_3Al in toluene as shown in Table 1. Dissolution of triisobutylaluminum (IBu_3Al) (Sigma Aldrich 257206 CAS 100-99-2), triisobutylamine (iBu_3N) (Sigma Aldrich 374989 CAS 1116-40-1), and benzene (Sigma Aldrich 319953) used in this study was performed in a glovebox under an Ar atmosphere and the toluene purified by distillation from sodium benzophenone ketyl under a nitrogen atmosphere and stored over 3 Å molecular sieves. To prepare samples for combustion experimentation consistent with strategies utilized for air-sensitive $[AlBrNEt_3]_4$ [6], ~0.5 mL are loaded into gastight syringes and sealed in bags with the syringe value closed under an Ar atmosphere. The 3 inch PTFE 1/16 inch OD x 0.040 in ID tubing syringe lead is flushed with nitrogen immediately before connecting to the sample delivery capillary and pumping the sample into the combustion experiment. A key benefit of IBu_3Al versus $[AlBrNEt_3]_4$ is its higher solubility limit and compatibility in toluene without ether co-solvent. As such, higher concentrations of IBu_3Al were tested herein: 280 mM, 440 mM, and 810 mM.

3. Results and discussion

Time-lapse images shown in Fig. 1 depict representative complete droplet lifetimes for each sample type at the highest concentration, unless noted otherwise. IBu_3N and the benzene control trials closely resemble the disruption-free burning of the toluene carrier fuel (the appearance midframe in the benzene trace of what appears to be a small disruption is an artifact caused by reflection off residue on the inside of the cover glass and was visible in the same location for every droplet imaged in that trial). Consistent with toluene/ether controls [6], small flashes occur upon termination of the control group droplets as a critical droplet size is reached and the remaining liquid fuel rapidly gasifies.

Four traces shown depict combustion behavior with IBu_3Al for the three concentrations tested including two profiles for the highest 810 mM loading. Generally for IBu_3Al, an initial disruption-free burning period precedes discrete strong and bright disruptions which have the potential to generate companion droplets, change the main droplet trajectory, and/or catastrophically disassemble the main droplet into smaller sub-droplets. As the concentration is increased from 280 mM to 440 mM, disruptions occur earlier and with more frequency, with neither concentration catastrophically dispersing the droplet with a single disruption event. At 810 mM loading however, a usual strong initial disruption commonly generates companion droplets while the main droplet survives, or catastrophically breaks the main droplet into several sub-droplets. The disruptive nature of the combustion with IBu_3Al additive is similar to microexplosions observed with ~10 mM $[AlBrNEt_3]_4$ in toluene/ether co-solvent [6].

To quantify the effect of the disruptive combustion behavior which emerges upon IBu_3Al addition, estimated burning rate constant enhancement are plotted in Fig. 2 versus additive concentration. While the control IBu_3N and benzene have slight negative to no effect on the burning rate constant relative to toluene (likely due to the higher boiling point of IBu_3N and lower combustion enthalpy of benzene relative to toluene), increases up to 61% are measured upon IBu_3Al addition, surpassing the ~20% increase measured with ~10 mM $[AlBrNEt_3]_4$ in toluene/ether [6]. IBu3N No conclusive difference in the burning rates is detected between 440 mM and 810 mM IBu_3Al despite the appearance of differing combustion disruption behavior. Notably, the standard deviation of the data collected increases substantially with the

Table 1
Samples tested with estimated burning rate constants and percent change relative to pure toluene control.

Sample	None K (mm^2/s)	280 mM K (mm^2/s)	% Δ	440 mM K (mm^2/s)	% Δ	810 mM K (mm^2/s)	% Δ
Toluene	2.33						
IBu_3Al		3.16	35	3.68	57	3.75	61
IBu_3N		2.28	−2.1	2.30	−1.4	2.28	−2.1
Benzene		2.21	−5.1	2.17	−7.0	2.27	−2.7

Fig. 1. Representative time-lapse images of free-falling droplets combusting with and without various additives. (A) Pure yoluene, (B) 810 mM IBu_3N in yoluene, (C) 810 mM benzene in toluene, (D–E) 280 mM and 440 mM IBu_3Al in toluene, (F–G) Two types of disruptions from 810 IBu_3Al in toluene. The mid-height emission expansion in (C) is an artifact caused by reflection off a spot of residue on the experiment cover glass and is not a disruption.

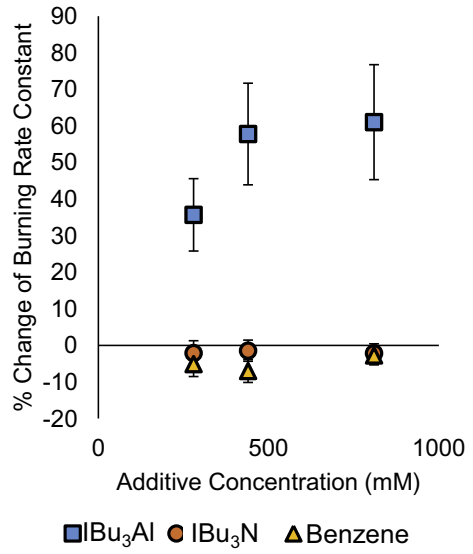

Fig. 2. Measured changes of burning rate constant relative to toluene (K = 2.33) with IBu_3Al, IBu_3N, and benzene additives. Error bars represent one standard deviation in each direction.

disruptive IBu_3Al additive, from 3.5% or less for control groups, to 10%, 14%, and 16% for 280 mM, 440 mM, and 810 mM IBu_3Al respectively, suggesting that the mechanism by which IBu_3Al increases burning rate is relatively stochastic either in occurrence or its effect on burning rate.

Multi-component liquid fuels are known to feature disruptive "microexplosion" events which can increase burning rate when the components have differing enough boiling points to superheat the lower boiling point fuel during droplet combustion [13–16]. Since the boiling point of IBu_3Al (359 K per Sigma Aldrich) is lower than that of toluene (384 K [17]), it is necessary to test a control additive with a similar boiling point (IBu_3N boiling point is 465 K [17]). Benzene has a boiling point (353 K [17]) close to that of IBu_3Al, but failed to generate combustion disruptions or affect the burning rate of toluene. This result suggests the mechanism of IBu_3Al activity is not due to superheated component microexplosions in the bi-component fuel.

To detail the nature of droplet disruptions and better assess the role of Al in the combustion, magnified color high-speed video of combusting droplets with accompanying pyrometric temperature estimation and concurrent emission spectroscopy between 474 nm and 502 nm wavelengths were collected for toluene, 810 mM IBu_3N in toluene, and 810 mM IBu_3Al in toluene. The spectroscopy is used to probe the combustion reactions for oxidation of gas-phase aluminum by detecting the $\Delta v = 0$ emission band of AlO near 484 nm [18, 19]. Resulting time-resolved imaging, flame temperature estimation, and AlO detection together reveal effects of disruptive events on the calorific output of the burn and liberation/participation of Al in combustion.

Figure 3 depicts select frames from magnified videos of IBu_3N control droplets. No difference is noticed between the magnified videos of toluene and IBu_3N controls, which both burn steadily without disruptions. Droplet disruptions caused by the IBu_3Al additive are shown in Fig. 4, in which the primary droplet survives, and Fig. 5, in which the main droplet is broken up into multiple companion droplets. Such disruptions are characterized by rapid release of gas phase reactants from the droplet which expand the flame zone and combust as they mix with ambient oxidizer and at times release companion droplets. Visible in the first two frames of Fig. 5 (and in supplemental video files), the additive also causes high frequency and low intensity flame perturbations throughout the droplet lifetime contrasting with the steady flame shape of the control samples (e.g. frame 5 of Fig. 3), suggesting continuous anisotropic and stochastic gas release from the droplets. Companion droplets released are visible in frames 5 and

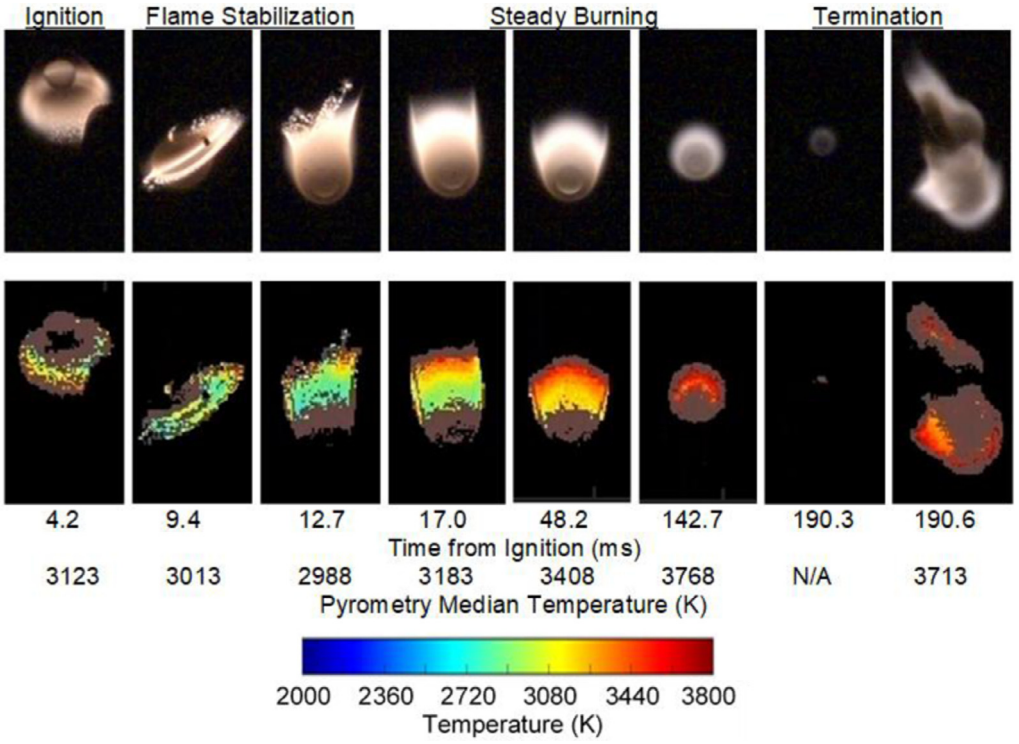

Fig. 3. Representative combustion profile from magnified videography and three-color spatial pyrometry of 810 mM IBu_3N control in toluene with time from ignition and median temperature noted per frame. Brown pixels in pyrometry images denote data points rejected for poor fit to theoretical color-channel ratios calculated by Eq. (2). (For interpretation of the references to color in this figure legend, the reader is referred to the web version of this article.)

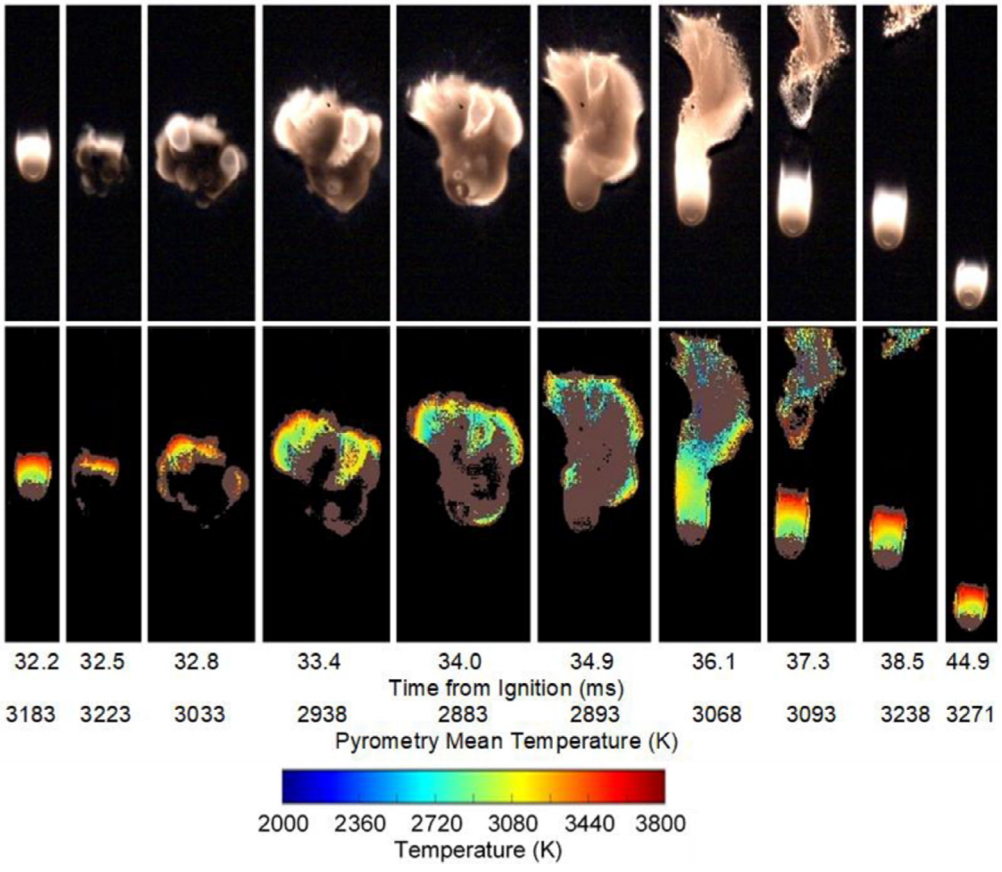

Fig. 4. Representative combustion disruption videography and pyrometric temperature estimates of 810 mM IBu_3Al in toluene in which the primary droplet survives intact with time from ignition noted per frame.

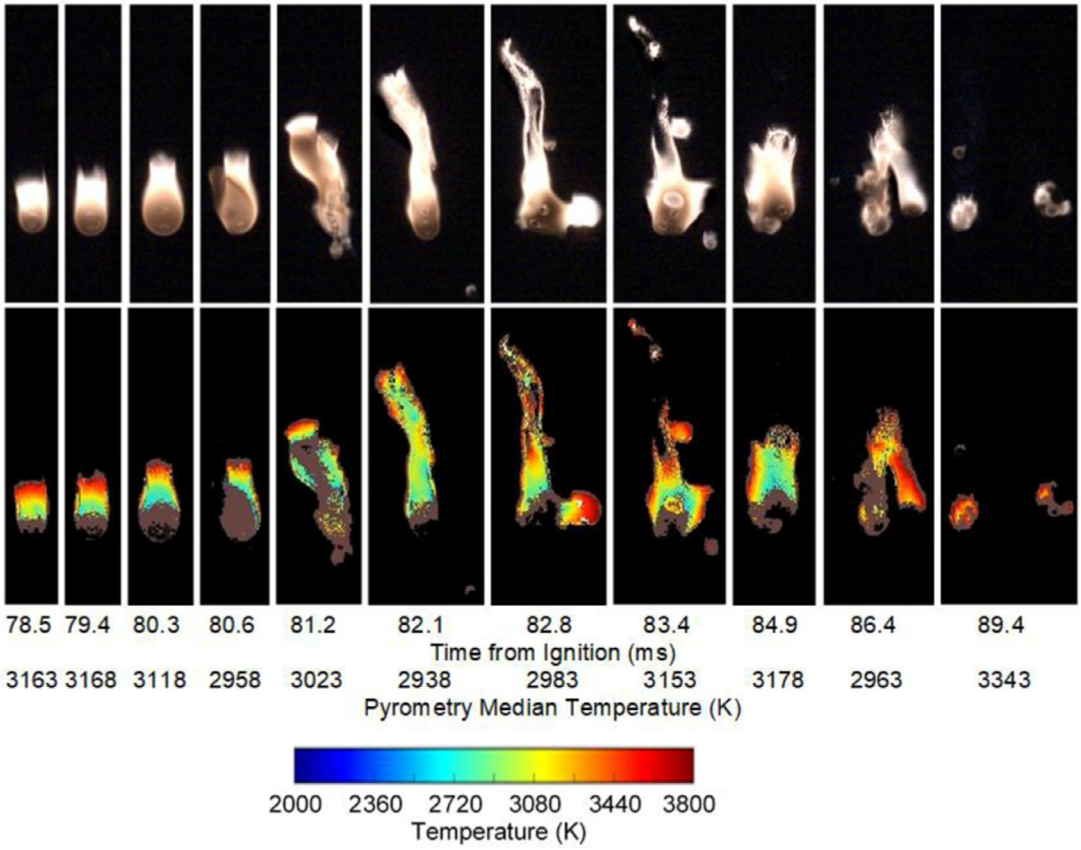

Fig. 5. Representative combustion disruption videography and pyrometric temperature estimates of 810 mM IBu_3Al in toluene in which the primary droplet is catastophically disassembled into sub-droplets with time from ignition noted per frame.

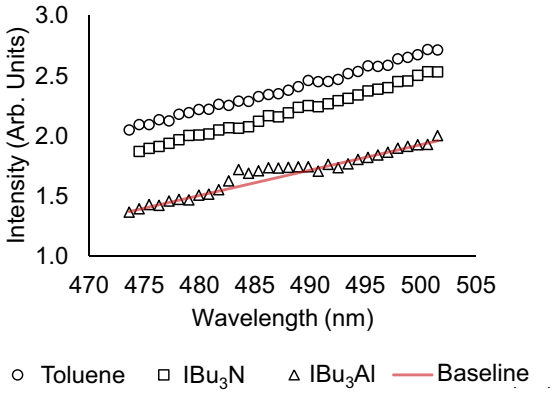

Fig. 6. Representative spectra collected from the emission of combusting droplets of toluene, IBu_3N in toluene, and IBu_3Al in toluene. Reference line is the least-squares fit of the IBu_3Al spectra omitting data between 433 nm and 439 nm. Data in that range is integrated over that baseline fit to measure AlO emission intensity.

6 of Fig. 4 showing the significant propensity of IBu_3Al to liberate sub-droplets during disruptions. Frames 2–4 in Fig. 5 also show substantial droplet swelling prior to the inception of the violent eruption and droplet breakup which resembles the cyclical inflation and eruption events seen with $[AlBrNEt_3]_4$ in [6] and nanoaluminum/nitrocellulose composite mesoparticles in kerosene in [9].

Representative emission spectra collected for toluene, IBu_3N, and IBu_3Al samples are shown in Fig. 6**.** Blackbody emission from soot particles comprises the majority of the radiation measured, however AlO atomic emission can be seen at a strong $\Delta v = 0$ emission band near 484–488 nm [18, 19]. The IBu_3Al emission spectra shown includes a departure from the blackbody emission at these wavelengths consistent with AlO emission. To estimate a time-resolved measure of AlO presence and relative strength, a least-squares polynomial fit is generated for each spectrum omitting data between 483 nm and 489 nm, and the area between this baseline and the measured data in this range was numerically integrated to estimate the intensity of the AlO peak in time. Plotting this AlO signal (overlaid with pyrometrically measured flame temperatures) in Fig. 8 shows that AlO emission was observed for IBu_3Al samples particularly near droplet gas eruptions, however no emission was detected in any toluene nor IBu_3N control trial, as shown in Supplemental Information. Gaps in AlO signals relative to flame temperature data are due to the smaller collection area of the spectrometer fiber relative to the camera field of view (spectroscopy collected from the upper 50% of the video frames).

Spatially averaged temperatures given by ratio pyrometry of the magnified color videos are also plotted versus droplet burning time in Figs. 7 and 8. As droplets burn and their flames shrink, this spatial average is biased towards the higher temperature regions as depicted in Fig. 3, leading to a linearly increasing mean temperature profile. A linear regression fit to the toluene control temperature after 23 ms (lower temperature prior to this time is during the droplet heat-up period) is shown in Fig. S1. This fit provides a basis of comparison of the temperature profiles across trials (reproduced as reference lines in Figs. 7 and 8) and is relatively repeatable for toluene as evidenced in Fig. S2. The flame temperature measured with IBu_3N control additive (which caused little to no burning rate change) in Fig. 7 is approximately 150 K greater than the toluene control throughout its lifetime owing to its higher

Table 2
Boiling points, stoichiometric combustion reactions and combustion energies for toluene, IBu_3N, and IBu_3Al fuels with oxygen.

Fuel	T_B (K)	Stoichiometric combustion reaction	ΔH_c (kJ/mol)
Toluene	383	$C_7H_8 + 9\ O_2 \rightarrow 7\ CO_2 + 4\ H_2O$	−3672
IBu_3N	465	$C_{12}H_{27}N + 18.75\ O_2 \rightarrow 12\ CO_2 + 13.5\ H_2O$	−7654
IBu_3Al	359	$C_{12}H_{27}Al + 19.5\ O_2 \rightarrow 12\ CO_2 + 13.5\ H_2O + 0.5\ Al_2O_3$	−8531
Benzene	353	$C_6H_6 + 7.5\ O_2 \rightarrow 6\ CO_2 + 3\ H_2O$	−3271

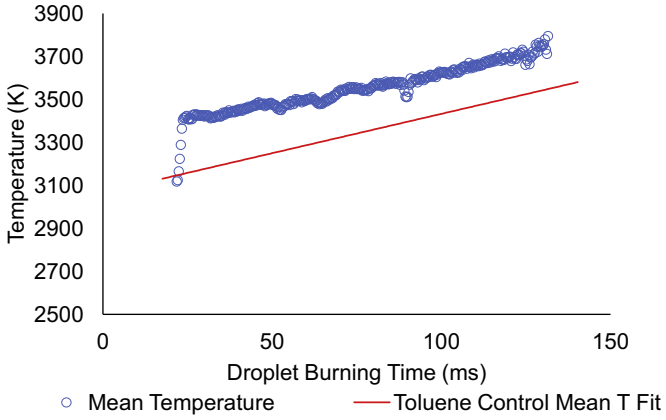

Fig. 7. 810 mM IBu_3N. Spatial mean of pyrometrically estimated temperature in magnified video "IBu_3N-1". Reference line corresponds to linear fit of toluene control temperature in Fig. S1. Plot overlay with integrated size of AlO emission peak sensed (zero AlO noise only) shown in Fig. S3.

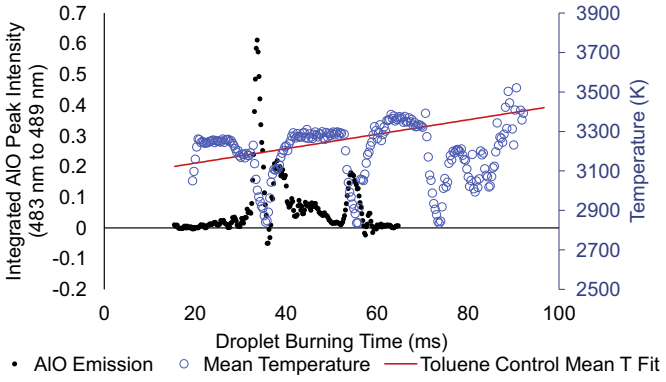

Fig. 8. 810 mM IBu_3Al. Spatial mean of temperature and integrated size of AlO emission peak sensed in magnified video "IBu_3Al-1". Reference line corresponds to linear fit of toluene control temperature in Fig. S1. Droplet leaves spectrometer view at 65 ms. Disruptions at 35 ms, 55 ms, and 73 ms.

boiling point and greater heat of combustion considering the reactions in Table 2, suggesting neither of these factors are to blame for the higher burning rates observed with IBu_3Al additive.

Figure S4 shows the pyrometrically estimated temperature profile and AlO emission signal for 810 mM IBu_3Al during ignition and heat-up. No AlO is detected in the first 10 ms of droplet burning. After the heat-up period, the droplet reaches a temperature approximately 50 K greater than the toluene control profile suggesting that even with the lower boiling point of IBu_3Al compared to toluene, its higher combustion heat as listed in Table 2 is ample to maintain a similar or slightly higher flame temperature than pure toluene droplets. The effect of disruptive microexplosions with IBu_3Al additive is evident in Fig. 8 wherein microexplosions occur at 35 ms, 55 ms, and 73 ms (and at 31 ms in Fig. S5), corresponding to sharp decreases in temperature as the flame mixes with cool ambient oxygen and prominent peaks in AlO emission indicating gas-phase Al combustion. The tapering-off of AlO detection events in Fig. 8 for consecutive disruptions seen in the flame temperature are due to the droplet leaving the smaller field of view of the spectrometer fiber relative to the video field of view used for pyrometry.

Similar to combusting droplet observations when $[AlBrNEt_3]_4$ clusters was added to toluene/ether in [6] and nanoaluminum/nitrocellulose composite mesoparticle were added to kerosene in [9], the primary effect of IBu_3Al addition appears to be the emergence of microexplosions/disruptions, characterized by rapid, violent release of gas phase products formed within the main droplet which combust as they reach the flame zone and can incite droplet break-up. Both droplet shape deformation and droplet break-up can increase gasification and burning rates as the surface area exposed to flame energy increases, as suggested in [9]. Rapid physical mixing of the vapor and liquid phases can also increase diffusion-limited reaction rates. The severe decreases in pyrometrically estimated flame temperatures during eruption events seen in Figs. 8 and S5 indicate strong mixing of the hot fuel-rich gases within the flame with the cool oxygen-rich atmosphere. As such, the burning rate increases observed upon IBu_3Al addition are likely caused by these violent droplet disruptions. Such events are unique to IBu_3Al-laden droplets in this study, with neither IBu_3N nor benzene additives able to cause similar eruptions, consistent with their lack of measured burning rate effects.

IBu_3Al is known to thermally decompose into aluminum, isobutene, and hydrogen and when this occurs in the presence of water, this process has been observed with evolution of AlO_X species above 300 K [20,21]. AlO spectroscopy in this study reveals that Al liberation is particularly strong at points of droplet microexplosions. Therefore, evolution of aluminum, isobutene and hydrogen within the droplet in this manner is a likely cause of the disruptive events, similar to the water-induced decomposition hypothesized previously for $[AlBrNEt_3]_4$ in toluene/ether droplets [6]. To assess the feasibility of such a mechanism, the volume of isobutene vapor available from one 600 µm toluene droplet of 280 mM IBu_3Al is estimated to be $\sim 3 \times 10^{-3}$ mL by the ideal gas law at 1 atm and 383 K (estimated droplet temperature) assuming 3 moles of C_4H_8 are available per mole of IBu_3Al, $C_{12}H_{27}Al$. Comparing this to the $\sim 1.1 \times 10^{-4}$ mL volume of such a droplet reveals that a theoretic gas evolution 26 times the volume of the droplet is available as isobutene vapor, which is more than ample to generate disruptive.

Like the mechanism set forth for $[AlBrNEt_3]_4$ cluster disruptions, water can also be considered as a diffusion-limited reactant of the gas generation reaction to estimate a time-scale to an initial disruption [6]. Assuming a 100 µm diameter sphere of isobutene in a 600 µm droplet of 280 mM IBu_3Al in toluene would cause a microexplosion, 5.5×10^{-12} moles of water are needed to react with IBu_3Al and generate 1.67×10^{-11} moles of isobutene. Following the analysis of [6] with a 600 µm diameter droplet saturated with water at its surface (0.33% water), a binary diffusion coefficient of 6×10^{-4} mol/(m^2-s), and a linear concentration gradient, enough water will reach one half-radius into the droplet to cause a microexplosion in approximately 30 ms. This closely resembles the time to the first microexplosions seen in Fig. 8.

4. Conclusions

The droplet combustion behavior of IBu_3Al dissolved in toluene has been investigated, revealing microexplosive droplet disruption events which are absent with pure toluene, IBu_3N in toluene, and benzene in toluene controls. Estimations of burning rate constants show the IBu_3Al additive increases toluene burning rates by 36%, 58%, and 61% with 280 mM, 440 mM, and 810 mM of IBu_3Al additive respectively while control additives have no appreciable effect. Direct observation of incited droplet microexplosions with pyrometric temperature estimation of color videos and concurrent measurement of AlO emission supports a mechanism proposed in which decomposition of IBu_3Al and reaction with water within the droplet evolves aluminum, isobutene, and hydrogen, inciting eruptions which increase the burning rate by physical mixing, droplet breakup, and droplet shape deformation. Drastic flame temperature decreases are indicative of the rapid mixing during these events while AlO emission sensed by spectroscopy shows that these microexplosions are also the primary vehicle by which aluminum enters the combustion reactions. This mechanism is similar to findings for $[AlBrNEt_3]_4$ in toluene/ether in [6] and nanoaluminum/nitrocellulose composite mesoparticles in kerosene in [9].

Acknowledgments

This work was made possible from the support of an Air Force Office of Scientific Research MURI grant.

Supplementary materials

Supplementary material associated with this article can be found, in the online version, at doi:10.1016/j.combustflame.2018.09.023.

References

[1] R.L. Zurawski, J.M. Green, An evaluation of metallized propellants based on vehicle performance, 23rd Joint Propulsion Conference (1987).
[2] P.R. Choudhury, Slurry fuels, Prog. Energy Combust. Sci. 18 (1992) 409–427.
[3] D.C. Mueller, S.R. Turns, Ignition and Combustion Characteristics of Metallized Propellants, Report No. NASA-CR-196850, National Aeronautics and Space Administration, Washington D.C., 1994.
[4] D. Sundaram, V. Yang, R.A. Yetter, Metal-based nanoenergetic materials: synthesis, properties, and applications, Prog. Energy Combust. Sci. 61 (2017) 293–365.
[5] R.A. Yetter, G.A. Risha, S.F. Son, Metal particle combustion and nanotechnology, Proc. Combust. Inst. 32 (II) (2009) 1819–1838.
[6] P.M. Guerieri, S. DeCarlo, B. Eichhorn, T. Connell, R.A. Yetter, X. Tang, Z. Hicks, K.H. Bowen, M.R. Zachariah, Molecular aluminum additive for burn enhancement of hydrocarbon fuels, J. Phys. Chem. A 119 (2015) 11084–11093.
[7] M.E. Gluckstein, Hypergolic Ignition Method Using Organoaluminum Compositions, U.S. Patent No. 3524317, 1970.
[8] P.M. Guerieri, R.J. Jacob, J.B. DeLisio, M.C. Rehwoldt, M.R. Zachariah, Stabilized microparticle aggregates of oxygen-containing nanoparticles in kerosene for enhanced droplet combustion, Combust. Flame 187 (2018) 77–86.
[9] P.M. Guerieri, J.B. DeLisio, M.R. Zachariah, Nanoaluminum/Nitrocellulose microparticle additive for burn enhancement of liquid fuels, Combust. Flame 176 (2017) 220–228.
[10] J.M. Densmore, M.M. Biss, K.L. McNesby, B.E. Homan, High-speed digital color imaging pyrometry, Appl. Opt. 50 (2011) 2659–2665.
[11] J. Kalman, T. Hedman, On the origin and use of the emissivity approximations for alumina particles, propellants, Explos. Pyrotech. 41 (2016) 793–797.
[12] R.J. Jacob, D.L. Ortiz-Montalvo, K.R. Overdeep, T.P. Weihs, M.R. Zachariah, Incomplete reactions in nanothermite composites, J. Appl. Phys. 121 (2017) 054307.
[13] C.K. Law, Internal boiling and superheating in vaporizing multicomponent droplets, AIChE J. 24 (1978) 626–632.
[14] C.K. Law, Recent advances in droplet vaporization and combustion, Prog. Energy Combust. Sci. 8 (1982) 171–201.
[15] A. Makino, C.K. Law, On the controlling parameter in the gasification behavior of multicomponent droplets, Combust. Flame 73 (1988) 331–336.
[16] C.H. Wang, X.Q. Liu, C.K. Law, Combustion and microexplosion of freely falling multicomponent droplets, Combust. Flame 56 (1984) 175–197.
[17] P.J. Linstrom, W.G. Mallard, eds., NIST Chemistry WebBook, NIST Standard Reference Database Number 69, National Institute of Standards and Technology, Gaithersburg MD, 20899, n.d. doi:10.18434/T4D303.
[18] C.G. Parigger, J.O. Hornkohl, Computation of AlO B 2 $\Sigma+\rightarrow$ X 2 $\Sigma+$ emission spectra, Spectrochim. Acta Part A Mol. Biomol. Spectrosc. 81 (2011) 404–411.
[19] C. Parigger, D.M. Surmick, A.C. Woods, A.B. Donaldson, J.L. Height, Measurement and analysis of aluminum monoxide flame emission spectra, 8th US National Meeting of the Combustion Institute (2013).
[20] B.E. Bent, R.G. Nuzzo, L.H. Dubois, Surface Organometallic chemistry in the chemical vapor deposition of aluminum films using triisobutylaluminum: β-hydride and β-alkyl elimination reactions of surface alkyl intermediates, J. Am. Chem. Soc. 111 (1989) 1634–1644.
[21] D.A. Kaplowitz, R.J. Jouet, M.R. Zachariah, Aerosol synthesis and reactive behavior of faceted aluminum nanocrystals, J. Cryst. Growth. 312 (2010) 3625–3630.